Ceramics International **21** (1995) 153–158

Influence of Polymerization on the Synthesis of $SrTiO_3$: Part II. Particle and Agglomerate Morphologies

E. R. Leite,[a] J. A. Varela,[b] E. Longo[a] & C. A. Paskocimas[a]

[a]Departamento de Química, UFSCar, PO Box 676, 13560 São Carlos, SP, Brazil
[b]Instituto de Química, UNESP, PO Box 355, 14800 Araraquara, SP, Brazil

(Received 15 February 1994; accepted 9 March 1994)

Abstract: Morphologies of $SrTiO_3$ particles and agglomerates synthesized by the traditional Pechini route and by the polymer precipitation route were characterized by the nitrogen adsorption/desorption technique and by transmission electron microscopy (TEM). A cluster structure of nanometric particles forming large agglomerates which are broken during pressing followed by cluster rearrangement was observed. The mean particle size is larger for $SrTiO_3$ obtained by the Pechini route and is related to the precursor thermal decomposition and particle growth during calcination. The particle growth is controlled by neck growth among particles and further motion of the particle boundary.

1 INTRODUCTION

In a previous paper[1] the influence of the polymerization route on the structure and thermal properties of polymeric precursors was analyzed. It was verified that the weight loss and temperature of $SrTiO_3$ phase formation depend on the excess of ethylene glycol.

Very few works correlate particle and agglomerate morphologies with the processing of the polymeric precursors. Lessing[2] suggested that unagglomerated powders cannot be obtained through calcination of a dense and rigid polymer precursor. Tai and Lessing[3] identify the need to control the ratio of ethylene glycol to citric acid to obtain soft porous precursors which are required to obtain free or weak agglomerate particles. Too much ethylene glycol or citric acid can retard the polymer expansion or promote complex reactions that otherwise affect it.

A recent study of strontium-doped lanthanum chromite examined the influence of the amount of polymeric gel on the particle morphology.[4] They found that too much polymer promotes the formation of strong agglomerates due to the excessive combustion heat generated during the burn-out of the organic material. This can lead to partial sintering of the agglomerates.

Too little polymer can lead to the formation of dense and rigid precursors which can form large particles and undesirable phases after calcination.

The control of particle morphology is one of the main objectives for the non-conventional synthesis method of ceramic powders. The characterization of particle morphology normally involves the measurement of specific surface area, and pore and particle size distribution by using the gas adsorption and desorption isothermal technique. The use of this technique provides the analysis of pore morphology,[5] surface area[6] and pore size distribution in agglomerates and porous solids.[8]

This work analyzes the influence of the precursor polymerization route on the $SrTiO_3$ particle and agglomerate morphologies. The $SrTiO_3$ particle processed by the traditional Pechini route (R1) and the polymer precipitation route (R2) were analyzed using the nitrogen adsorption and desorption techniques, as well as by transmission electron microscopy (TEM), and by measuring the crystalline size by X-ray diffraction (XRD).

Ceramics International 0272-8842/95/$9.50

2 EXPERIMENTAL PROCEDURE

The $SrTiO_3$ powders were prepared using two different routes as described elsewhere.[1] In the traditional Pichini route (R1), the polyester resin is polymerized at 250°C, milled and further calcined at 700°C for 3 h. In the polymer precipitation route (R2), the polymer is precipitated in acetone solution, washed in acetone and further calcined at 700°C for 3 h. Both R1 and R2 materials were ground in a ball mill with ethanol for 4 h. The powders were then characterized by XRD showing a single $SrTiO_3$ phase.

To analyze the powders by TEM, the particles were dispersed in ethanol by ultrasonic vibration for 30 s and then supported on copper screen covered by polymeric film using a 100 kV microscope. For nitrogen adsorption/desorption analysis the samples were degassed in He atmosphere and in vacuum at 250°C for 30 min. Pore size distributions by nitrogen desorption were determined using the BJH method.[7,9] To determine the existence of micropores, the curve of adsorbed volume (V) versus statistical thickness of the adsorbed layer (t) were found using the De Boer equation,[10]

$$\mathrm{Log}_{10}(P/P_0) = D/t^n + E\exp(-Ft) \qquad (1)$$

where D, E and F are empirical constants related to the adsorption heat and the liquefaction latent heat of the gas, P is the pressure, P_0 is the saturation pressure and t is the thickness of the adsorbed layer. For solids without micropores (pores smaller than 2 nm), $V \times t$ is a linear relation. The surface area was determined by using the BET multi-points method,[6] and an ASAP 2000 (Micromeretics), was used for the adsorption/desorption analysis.

The crystallite sizes (D) were determined using the diffraction peak of the (211) plane of $SiTiO_3$ and the Sherrer equation,

$$D = 0{\cdot}9\lambda/(\beta.\cos\theta) \qquad (2)$$

where λ is the wavelength (Cu Kα) and β is the corrected half-width of the diffraction peak. In this study it was considered that

$$\beta = (B^2_{obs} - b^2)^{1/2} \qquad (3)$$

where B_{obs} is the line width at half-peak intensity related to $SrTiO_3$ and b is the line width of the internal standard (plane (004) of metallic silicon).

To analyze the agglomerate morphology the green density was determined by mercury picnometer, and the shrinkage of pellets isostatically pressed at 220 MPa. The shrinkage was determined as function of initial diameter of the green pellet pressed uniaxially before the isostatic pressing. The pore size distribution was also determined by nitrogen adsorption/desorption for the pressed pellets.

The calcination parameters for the polymeric precursors were chosen to be 700°C for 3 h, because after calcination of the precursor obtained by route R2 no more weight loss was observed. The powder obtained by route R1 was calcined using the same parameters, even though this is not the best calcination temperature for this powder.

3 RESULTS AND DISCUSSION

3.1 Powder morphology before pressing

The plot of Fig. 1. shows the nitrogen adsorption/desorption curves for the powders obtained by routes R1 and R2. The analysis of this plot shows an isotherm of type II,[11] indicating the presence of mesopores (pores with a diameter of 2–100 nm) and a hysterese H-1.[5] The hysterese H-1 suggests the presence of agglomerates with open cylindrical pores for both powders.

Figure 2 shows the plot of adsorbed volume as a function of the statistical thickness of the

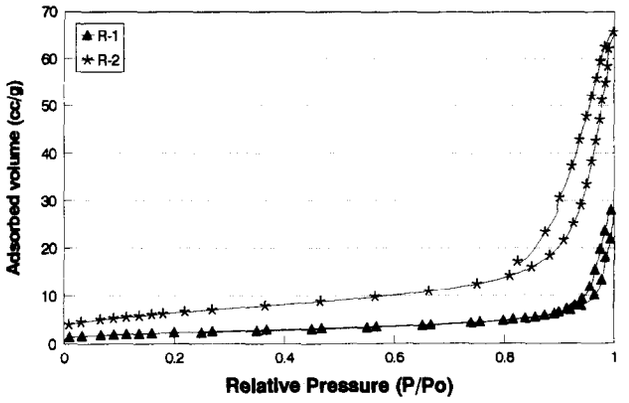

Fig. 1. Nitrogen adsorption/desorption isotherm for R1 and R2 powders.

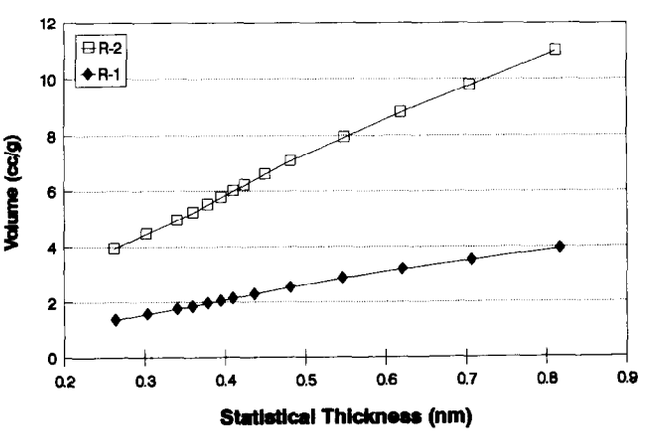

Fig. 2. Adsorption volume as function of the statistical thickness of the adsorbed layer for R1 and R2 powders.

absorbed layer (t). In this plot a linear behavior is observed for both powders R1 and R2, indicating that there are no micropores (pores smaller than 2 nm) in either system.

Given this lack of micropores the BJH method[7,9] was then used to determine the pore size distributions for mesopores of both R1 and R2 powders. Figure 3 shows a wide pore size distribution for both powders. However, the R2 powder has a smaller mean pore diameter (16 nm) than that of the R1 powder (80 nm). This difference is basically related to the mean particle size. Table 1 show results of surface area (S_{BET}), particle size obtained by surface area (D_{BET}), crystallite size (D), and mean particle size by TEM (D_{TEM}). The mean particle size obtained from surface area was calculated based on the equation

$$D_{BET} = 6/\rho_t.S_{BET} \quad (4)$$

where ρ_t is the theoretical density of $SrTiO_3$ (5·12 g/cm^3). The analysis of this table shows that the R2 powder has a smaller particle size than powder R1. Compacts obtained from powders with small mean particle size have a small mean pore size.

Figures 4(a) and (b) are the TEM micrographs of the R1 powder, which show equiaxial particles forming elongated agglomerates. Figure 4(a) also shows series of defects in the particles, such as dislocations (D), internal pores (E), and pores among particles (A,B), and Fig. 4(b) shows fissures (F) as well as necks between particles (C).

Figures 5(a) and (b) are TEM micrographs of the R2 powder. Figure 5(a) shows two populations of pores, one with pore size about 70 nm (B) and other about 10 nm (A). Well-defined necks between particles (C), fissures (F) and dislocations (D) are also clearly visible.

Table 1 shows that the mean particle size obtained by TEM (D_{TEM}) is smaller than that

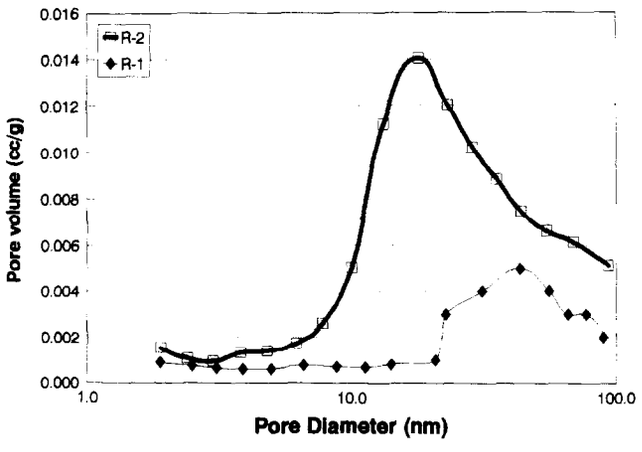

Fig. 3. Pore size distribution curves obtained from desorption of nitrogen for R1 and R2 powders.

Table 1. Morphologic characteristics of the $SrTiO_3$ particles processed by routes R1 and R2

Sample	S_{BET} (m^2/g)	D_{BET} (nm)	D (Crystallite) (nm)	D_{TEM} (nm)
R1	8·4	140	45	62 ± 9
R2	23·3	50	16	32 ± 6

obtained by the nitrogen adsorption method (D_{BET}) for both powders. Introducing the concept of an agglomeration factor (AF), defined as

$$AF = D_{BET}/D_{TEM} \quad (5)$$

leads to a calculated value of 2·2 for the R1 powder and 1·6 for the R2 powder. This means that the gas adsorption should be considered two particles in average. This is confirmed by the presence of necks between particles observed in Figs 4 and 5. During the nitrogen adsorption, then, a single layer of nitrogen molecules forms over several particles, not over an individual particle.

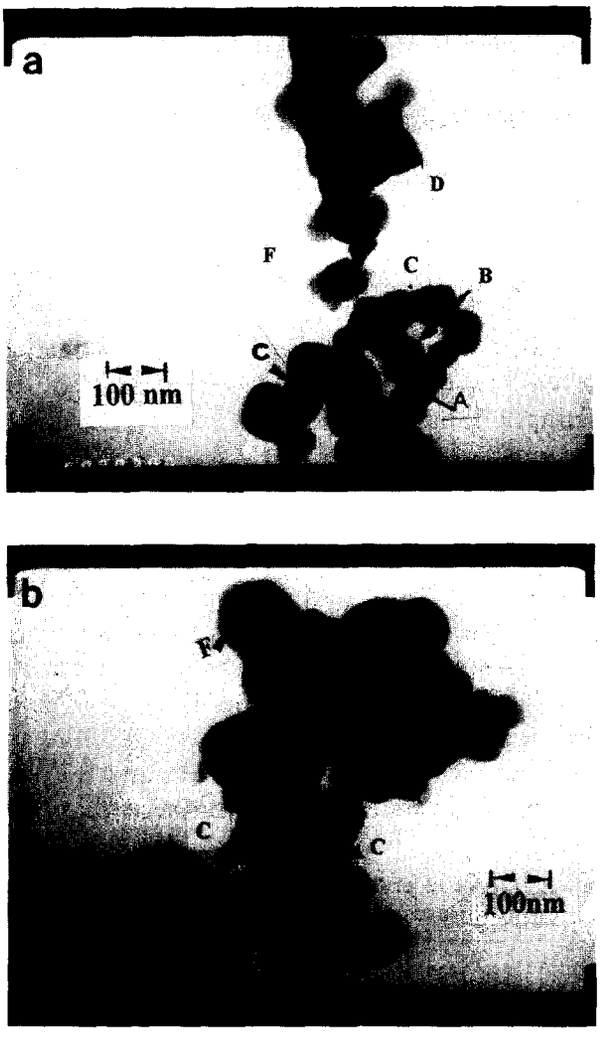

Fig. 4. (a) and (b) TEM micrographs of the $SrTiO_3$ powder processed by route R1.

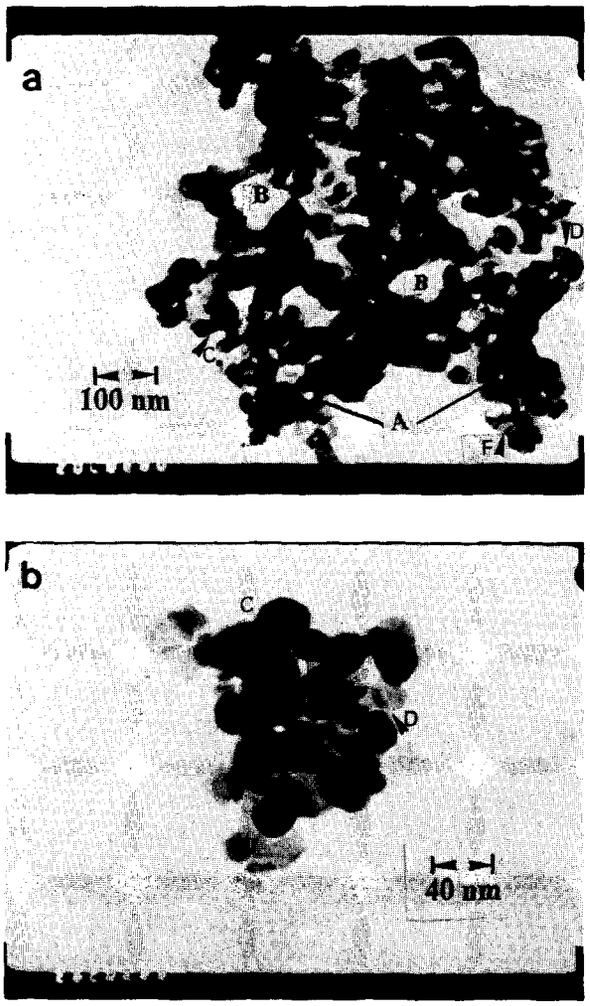

Fig. 5. (a) and (b) TEM micrographs of the $SrTiO_3$ powder processed by route R2.

TEM and nitrogen adsorption/desorption results show that the morphology of R1 and R2 powders is similar; however, the particle sizes are different due to the thermal decomposition step of the starting R1 and R2 materials.

3.2 Powder morphology after pressing

Table 2 shows the data of green density and shrinkage after isostatic pressing of both the R1 and R2 powders. These results show that large shrinkage occurs after isostatic pressing (from 7 to 11%), indicating that during pressing the agglomerates break and the particles rearrange. Pore size distribution for pressed pellets of R1 and R2 powders were determined by nitrogen adsorption/desorption and the BJH method. In Figs 6 and 7, the plots of particle size distribution of the powder and the compact are compared. The $SrTiO_3$ pressed pellet obtained from route R1 (Fig. 6) shows a narrowing of pore size distribution, with elimination of pores larger than 70 nm. A bimodal pore size distribution is then formed, with one most frequent pore of 40 nm and another of 55 nm.

Table 2. Values of green density and shrinkage after isostatic pressing of R1 and R2 powders

Sample	Relative green density (%)	Shrinkage after pressing (%)
R1	53	7·9
R2	44	11·9

For the $SrTiO_3$ powder obtained from route R2, an elimination of pore size larger than 70 nm when the pellet is isostatically pressed is observed. A bimodal pore size distribution is also formed for this power, with one most frequent pore of 17 nm and another of 28 nm. No change in pore volume was observed after pressing for either power.

These results indicate that during pressing, the large pores, between nanometric particle clusters, are broken (pore B of Figs 4(a) and 5(a)). New pore size population is created with a mean size of the same order of magnitude of the mean particle size (D_{TEM}). The small size alteration of pores smaller than D_{TEM} indicates that these pores are formed by partially sintered particles (indicated by A in Figs 4(a) and 5(a)).

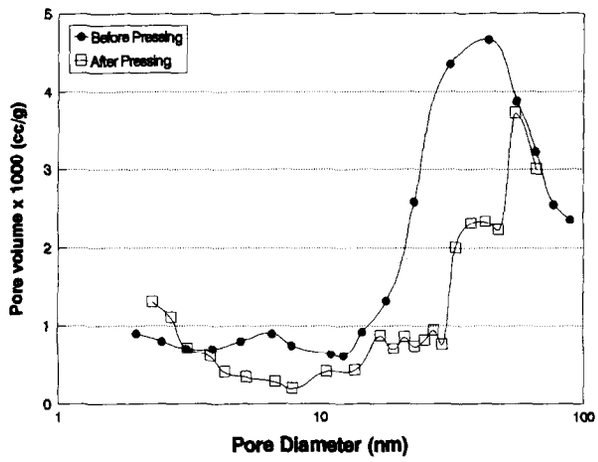

Fig. 6. Pore size distribution curves obtained from desorption of nitrogen for R1 powder before and after isostatic pressing.

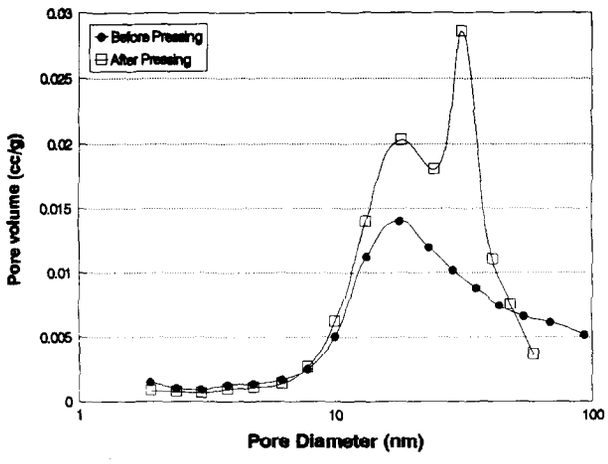

Fig. 7. Pore size distribution curves obtained from desorption of nitrogen for R2 powder before and after isostatic pressing.

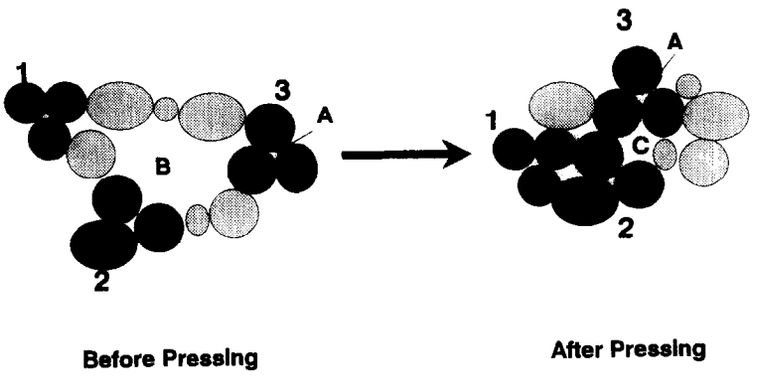

Fig. 8. Qualitative model showing the changes provided by isostatic pressing in R1 and R2 powders.

Figure 8 describes qualitively the alterations in agglomerate morphology after pressing the R1 and R2 powers. In this diagram it is observed that pressing causes the agglomerates to rupture. The large pore population of 100 nm (pore B) disappears by rearrangement of the smaller particle clusters (marked 1–3 in this figure). A new pore population (indicated by C) then forms with mean size equivalent to mean particle size. Small pores (A) are not altered, due to elevated mechanical resistance of the agglomerate.

This model, based on rupture of agglomerates and rearrangement of clusters, can explain the changes that occur in the pore size distribution curves after the ultrafine $SrTiO_3$ powders obtained from routes R1 and R2 are pressed, and can also explain the large shrinkage of the pellets after isostatic pressing. Similar behavior was observed by Van de Graaf *et al.*[12] during pressing of ultrafine ZrO_2–Y_2O_3 powder.

3.3 General discussion

The presented results show that the $SrTiO_3$ powders processed by routes R1 and R2 have similar morphology for particles and agglomerates. However, the mean particle size of the R1 powder is larger than the R2 powder. Since the nucleation of the $SrTiO_3$ starts first in the R1 starting material and the same calcination temperature is used for decomposition of both starting materials, the particle growth rate for the R1 powder should be higher than that for the R2 powder. Table 1 shows that the crystallite size is larger for the R1 powder. The value for crystallite size and the presence of internal pores and fissures in the particles are indicative that the particle growth rate is higher in the R1 powder than in the R2 powder.

The TEM micrographs of Figs 9(a) and (b) show elongated particles and particle boundary motion in the direction of smaller particles (marked A in Fig. 9(a)). These figures suggest that the particle growth is controlled by the displacement of particle boundaries. Similar mechanism of particle growth was observed by Greskovich and Lay[13] in Al_2O_3 porous compact. According to Greskovich and Lay[13] the particle or grain growth start by neck growth between the grains until the grain boundary is free to move. The grain boundary motion is fast compared to neck growth, and when the neck reaches a size comparable to the grain size the boundary will move rapidly toward the smaller grain in a continuous process involving smaller neighbor particles. Surface diffusion

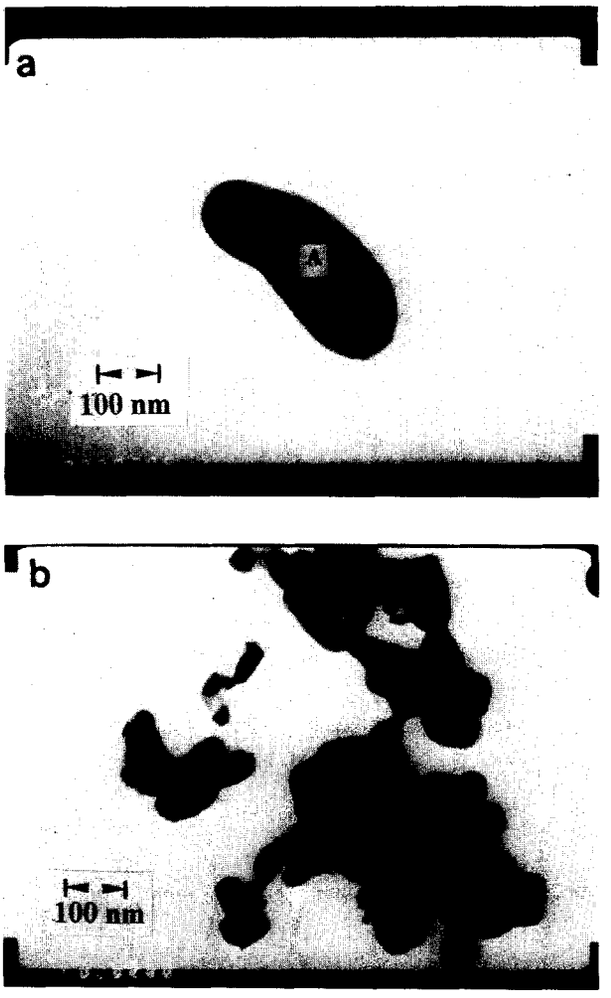

Fig. 9. TEM micrographs of (a) R1 and (b) R2 powders.

and evaporation–condensation probably promote neck growth between particles. Tai and Lessing[4] also considered that the growth mechanisms for the strontium-doped lanthanum chromite particles processed by polymeric route are related to surface diffusion or evaporation–condensation. This particle growth mechanism should start in the clusters of nanometric particles originating larger particles with defects such internal pores, fissures, and dislocations.

Besides the elevated calcination temperature, the high weight loss of the R1 starting material should also contribute to the larger particle growth. This high weight loss leads to an increase of the local temperature due to combustion heat of the excess organic material which promotes partial sintering of the particle clusters.

4 CONCLUSION

The choice of calcination parameters is fundamentally important if fine particles free of agglomerates are to be obtained through the polymeric precursor method. During the calcination process, strong or weak agglomerates can form among the clusters of nanometric particles. These agglomerates of particle clusters are broken during pressing process. Particle growth during calcination is probably due to neck growth between particles and further motion of the particle boundary.

ACKNOWLEDGEMENT

The authors acknowledge the financial support of the FAPESP, FINEP and CNPq.

REFERENCES

1. LEITE, E. R., SOUSA, E., LONGO, E. & VARELA, J. A., Influence of polymerization in the synthesis of $SrTiO_3$: part I, characteristics of the polymeric precursors and its thermal decomposition. *Ceram. Int.* (1994) (submitted).
2. LESSING, P. A., Mixed-cation oxide powders via polymeric precursors. *Ceram. Bull.*, **68**(5) (1989) 1002–7.
3. TAI, L. W. & LESSING, P. A. Modified resin-intermediate processing of perovskite powders: part I: optimization of polymeric precursors. *J. Mater. Res.*, **7**(2) (1992) 502–10.
4. TAI, L. W. & LESSING, P. A., Modified resin-intermediate processing of perovskite powders: part II: processing for fine, non agglomerated Sr doped lanthanum chromite powders. *J. Mater Res.*, **7**(2) (1992) 511.
5. SING, K. S. W., Reporting physisorption data for gas/solid systems with special reference to the determination of surface area and porosity. *Pure Appl. Chem.*, **54**(11) (1982) 2201–18.
6. BRUNAUER, S., EMMETT, P. H. & TELLER, E., Adsorption of gases in multi molecular layer. *J. Am. Chem. Soc.*, **60** (1938) 309–19.
7. BARRET, E. P., JOYNER, L. G. & HALENDA, P. P., The determination of pore volume and area distribution in porous substances. I, computation from nitrogen isotherms. *J. Am. Chem. Soc.*, **73** (1951) 373–80.
8. HENNINGS, D. & SCHREINEMACKER, S., Characterization of hydrothermal barium titanate. *J. Eur. Ceram. Soc.*, **9** (1992) 41–6.
9. *Operation manual, ASAP 2000.* Micrometrics Instrument Corp., Nocross, GA, USA (1991)
10. de BOER, J. H., LINSEN, B. G. & OSINGA, J. J., Studies on pore systems in catalyst: VI, the universal *t*-curve. *J. Catal.*, **4** (1965) 643–8.
11. BRUNAUER, S., DENING, L. S., DENING, W. S. & TELLER, E., A theory of the Van der Walls adsorption of gases. *J. Am. Chem. Soc.*, **62** (1940) 1723–32.
12. Van de GRAAF, M.A.L.G., TERMAAT, J. H. H. & BURGGRAAF, A. J., Microstructure and sintering kinetics of highly reactive ZrO_2–Y_2O_3 ceramics. *J. Mater. Sci.*, **20** (1985) 1407–18.
13. GRESKOVICH, C. & LAY, K. W., Grain growth in very porous Al_2O_3 compacts. *J. Am. Ceram. Soc.*, **55**(3) (1972) 142–6.